

Jamming, relaxation, and memory in a minimally structured glass formerPatrick Charbonneau^{1,2} and Peter K. Morse^{1,3,4,5,*}¹*Department of Chemistry, Duke University, Durham, North Carolina 27708, USA*²*Department of Physics, Duke University, Durham, North Carolina 27708, USA*³*Department of Chemistry, Princeton University, Princeton, New Jersey 08544, USA*⁴*Department of Physics, Princeton University, Princeton, New Jersey 08544, USA*⁵*Princeton Institute of Materials, Princeton University, Princeton, New Jersey 08544, USA*

(Received 25 April 2023; accepted 3 October 2023; published 3 November 2023)

Structural glasses form through various out-of-equilibrium processes, including temperature quenches, rapid compression (crunches), and shear. Although each of these processes should be formally understandable within the recently formulated dynamical mean-field theory (DMFT) of glasses, the numerical tools needed to solve the DMFT equations up to the relevant physical regime do not yet exist. In this context, numerical simulations of minimally structured (and therefore mean-field-like) model glass formers can aid the search for and understanding of such solutions, thanks to their ability to disentangle structural from dimensional effects. We study here the infinite-range Mari-Kurchan model under simple out-of-equilibrium processes, and we compare results with the random Lorentz gas [J. Phys. A **55**, 334001 (2022)]. Because both models are mean-field-like and formally equivalent in the limit of infinite spatial dimensions, robust features are expected to appear in the DMFT as well. The comparison provides insight into temperature and density onsets, memory, as well as anomalous relaxation. This work also further enriches the algorithmic understanding of the jamming density.

DOI: [10.1103/PhysRevE.108.054102](https://doi.org/10.1103/PhysRevE.108.054102)**I. INTRODUCTION**

The free-energy landscape analogy has long been used to conceptually unify the structure, dynamics, and thermodynamics of supercooled liquids and glasses [1–4]. A roughening terrain, for instance, suggests why liquids should become sluggish upon cooling and then rigidify as one of many disordered metastable states. The intuitive nature of this representation has further found broad uses in fields ranging from ecology [5,6] to general relativity [7]. For certain abstract models, the metaphor has even been shown to be exact [8,9]. The equilibrium and out-of-equilibrium dynamics of fully connected p -spin glass models, in particular, can be understood in terms of specific landscape features [10–17]. The extension of the analogy to finite-size systems is also still actively pursued [18–20].

Following the success of this approach, a similar theoretical program has been initiated for models that are conceptually closer to structural glasses. After theoretically solving for a number of static features of *simple glasses* in the high-dimensional, $d \rightarrow \infty$ limit [21,22], a formal dynamical mean-field theory (DMFT) description of these models has been formulated [23–27]. While symmetries of the resulting equations have been exploited to show the equivalence of response to various perturbations in both mean-field theory [28] and low dimensions [29], actual solutions of these equations are currently only available over relatively narrow equilibrium [30,31] and low density [32] conditions. The physical robustness of various finite- d features of the

landscape thus remains unclear. In particular, although the theoretical description of jammed hard spheres captures the remarkable criticality of systems as low as $d = 2$ [33–35], key features of the out-of-equilibrium processes that bring systems to jamming remain somewhat murky.

From a landscape perspective, one of the simplest out-of-equilibrium processes to consider is to instantaneously quench a liquid (or crunch hard spheres) equilibrated at a given temperature (or density) to its inherent state (IS), sometimes called the inherent structure [36]. However, the dynamics of that relaxation [16,37–41], the IS algorithmic robustness [39,42], and its memory of the initial density [43–47] or temperature [3,17,48–51] are incompletely described. For hard spheres, even the lowest density at which jammed (disordered) states can be obtained remains unclear. Finite- d results have been obtained [47,52–54], and for some of these features, a reasonably robust phenomenology has been observed. Yet the significant influence of liquid structure in low- d systems over the accessible dimensional range [55,56] obfuscates what the DMFT description might be. A different way to extrapolate to $d \rightarrow \infty$ —and therefore to assess the robustness of the mean-field description as well as to extract physical insight from it—is to consider the d convergence of models that exhibit a markedly simpler structure.

In this spirit, Manacorda and Zamponi have recently considered the jamming behavior of the simple random Lorentz gas (RLG) [40], which is defined by the dynamics of an individual tracer particle moving in a system of fixed obstacles, distributed uniformly at random. By construction, the RLG model is formally equivalent to simple glasses in the limit $d \rightarrow \infty$, up to a trivial scaling factor (described below) [57,58]. Given the single-particle nature of this model, its

*Corresponding author: peter.k.morse@gmail.com

relaxation dynamics can be cleanly integrated, which currently enables numerical simulations up to $d = 22$. Interestingly, this analysis has revealed unexpected features of the gradient dynamics. While unjammed systems reach an IS in a fairly short time, jammed systems appear to drift sublogarithmically with time toward an IS, thus calling into question the traditional algorithmic approach to jamming, which relies on fixing cutoffs for determining convergence. Surprisingly, the study obtained a significantly lower jamming density than had been previously reported for an analogous system (Ref. [22], Fig. 9.2).

To assess the robustness of these findings, we consider a natural complement to the single-particle RLG, namely the many-body Mari-Kurchan (MK) model [59], which consists of N particles interacting via uncorrelated shifts chosen uniformly at random. By construction, this model also exhibits a trivial structure in all d and is described by the same DMFT equations as the RLG in the limit $d \rightarrow \infty$. It should therefore have the same jamming properties as the RLG in that limit. Although preliminary work has been done to address the jamming behavior of the MK model [22,59], a comprehensive finite-size and finite-dimensional analysis is still lacking. In addition, the jamming algorithms used thus far are not straightforwardly amenable to theoretical analysis as they mix quenching with equilibrating. In this work, we provide such analysis and undertake a comparison to the relaxation dynamics of the RLG. While we validate many of the RLG findings, we find its estimate of the jamming density to be much lower than what any standard jamming algorithm can produce for the MK model. This effort additionally allows us to characterize the IS memory and to conclusively determine that its onset transition, at which the IS starts depending on the initial condition, does not coincide with the dynamical transition, as it does in the pure p -spin model [14].

The rest of this article is structured as follows. Section II reviews relevant definitions for the various quantities associated with jamming considered in this work. Section III presents the numerical MK planting techniques, gradient descent, and jamming algorithms. Section IV summarizes known results about the threshold and dynamical transition in MK systems. Section V A reports the relaxation dynamics in harmonic MK systems across spatial dimension and compares those results with RLG results. Section V B then discusses jamming in both soft and hard sphere MK models. For the former, we specifically relate the findings to the RLG and to prior theoretical predictions. The existence of IS memory in both soft and hard sphere MK models is considered in Sec. V C. Section VI concludes by discussing the implications of these results for generic solutions of the DMFT and for more physical models of glasses in finite d .

II. DEFINITIONS

In this section, operative definitions for several of the terms and quantities used throughout this work are provided. Each system contains N spheres in dimension d with a packing fraction ϕ , which will in some cases be varied.

Rattler: A particle whose motion is not fully constrained by other particles in an otherwise jammed system. A standard method for identifying a rattler is determining whether its

center lies on the convex hull of the union of its center and the points of contact with other particles [54,60–62]. Note that this definition and the algorithm are necessarily recursive.

Isostaticity: A system in which every nonrattling particle is fully constrained with no excess constraints (states of self-stress). In the thermodynamic limit of $N \rightarrow \infty$, a simple mechanical stability argument by Maxwell [34,63] states that the average number of contacts per nonrattling (hard) particle is $2d$. More specifically, finite-size systems with a finite bulk modulus require the average number of contacts per nonrattling particle to be $2d - 2d/N + 2/N$ (see Ref. [64] for more details). Such systems are sometimes called *iso + 1*.

Jamming: A hard sphere system that is isostatic and mechanically stable is jammed. Soft sphere systems are deemed jammed if they are isostatic or if they have additional constraints beyond *iso + 1* (and are therefore hyperstatic).

Inherent state (IS): A jammed state of an initial configuration found by an ideal crunch. Such a crunch is devoid of processes that raise the jamming density, such as thermalization and rearrangements [4,36,65]. The inherent state is therefore the lowest jammed density achievable through bulk physical processes involving monotonic compression or dilation [66].

Jamming threshold: In mean-field theory, the density at which jammed states appear in sufficient number for a finite complexity to be computed (see Refs. [8,67] and Ref. [22], Sec. 7.4.3).

Dynamical transition: In the mean-field limit of $d \rightarrow \infty$, a hard sphere fluid is only ergodic up to the dynamical transition density ϕ_d [21]. In finite d the dynamical transition is avoided, and states beyond ϕ_d have a finite lifetime, at least up to the putative Kauzmann transition ϕ_K [21].

State following transition: For hard sphere fluids equilibrated above the state following density, a clear separation of timescales between slow compression and structural relaxation allows for a quasiequilibrium mapping to the inherent state [22,68].

III. COMPUTATIONAL METHODS

In this section, we describe the various computational approaches employed for obtaining IS of a MK fluid. We first detail how to obtain efficiently equilibrated harmonic sphere configurations. We then present a gradient descent scheme for soft spheres and two different hard sphere crunching algorithms:

(i) *Gradient descent (GD)*: Soft particles are initially allowed to overlap with a Hookean contact potential, and the energy is minimized via a steepest descent algorithm. The only free parameter, ϵ , controls the timescale for the smallest step, set by the change in gradient.

(ii) *Effective potential (EP)*: An iteration between particle expansion and minimization of an effective attractive potential between hard spheres. The hard sphere condition is therefore maintained throughout. These two steps are balanced through the use of two free parameters, θ and τ , which represent the growth rate and the number of minimization steps, respectively.

(iii) *Event driven (ED)*: Hard particles are inflated following an overdamped dynamics, thus providing contact forces, and hence equations of motion.

Each of these algorithms approximates an ideal crunch differently, and therefore offers a distinct estimate of the jamming line, and in particular of its low-density start, φ_{J0} .

A. Planting for radially symmetric soft potentials

Equilibrium MK configurations can generically be planted under any conditions, thus markedly reducing the computational cost of initializing systems. While hard spheres can be planted by simple rejection sampling [59,69], more care is needed for systems with soft interactions. We describe here the process for a generic contact pair interaction with power-law exponent $\alpha > 1$. (The rest of this work only considers harmonic spheres with $\alpha = 2$.) The total energy U is then the sum of all pair energies u for particles i and j , $U = \sum_{ij} u(h_{ij})$, with

$$u(h_{ij}) = \frac{\varepsilon}{\alpha} (-h_{ij})^\alpha \Theta(-h_{ij}), \quad (1)$$

where $\varepsilon = 1$ sets the energy scale, Θ is the Heaviside function, and

$$h_{ij} = d \left(\frac{|\mathbf{r}_i - \mathbf{r}_j + \mathbf{\Lambda}_{ij}|}{\sigma} - 1 \right) \quad (2)$$

is the dimensionless gap for monodisperse spherical particles of diameter σ at positions \mathbf{r}_i with random pair offset $\mathbf{\Lambda}_{ij}$. The factor d ensures that the potential remains finite when $d \rightarrow \infty$ [21,40,70]. For this family of systems, the random offset $\mathbf{\Lambda}_{ij}$ needs to be generically chosen from the probability distribution

$$P(\mathbf{\Lambda}_{ij}|\mathbf{r}_{ij}) = \frac{\exp[-\beta u(|\mathbf{r}_{ij} + \mathbf{\Lambda}_{ij}|)]}{\int d\mathbf{\Lambda}_{ij} \exp(-\beta u(|\mathbf{r}_{ij} + \mathbf{\Lambda}_{ij}|))} \\ = \frac{\exp[-\beta u(|\mathbf{r}_{ij} + \mathbf{\Lambda}_{ij}|)]}{V_b - V_d \sigma^d \left[1 - d \int_0^1 \xi^{d-1} e^{-\frac{d\alpha}{\alpha} (1-\xi)^\alpha} d\xi \right]} \quad (3)$$

at inverse temperature $\beta = \frac{1}{k_B T}$ (with Boltzmann constant k_B hereon set to unity) in a simulation box of volume V_b , where $V_d = \frac{\pi^{d/2}}{\Gamma(1+d/2)}$ is the volume of a d -dimensional unit sphere. For $d^\alpha \beta/\alpha \rightarrow \infty$ the hard sphere MK model is recovered, and for $d^\alpha \beta/\alpha \rightarrow 0$ the ideal gas limit is recovered. Note that the above expressions are independent of the simulation box geometry. We specifically use simulations boxes here under D_d boundary conditions (based on the d -dimensional generalization of the $d = 3$ face-centered-cubic lattice) in order to most efficiently sample systems of N particles [56,71,72].

Prior simulations of the soft sphere MK model have sampled this distribution using the Metropolis-Hastings algorithm [39,73], but both speed and accuracy can be improved by using inverse transform sampling (ITS) (Ref. [74], Chap. 2.2). Given the total probability that particle i is contained within a distance σ of j , $P(r_{ij} < \sigma) = d \times V_d \int_0^{\sigma} dq q^{d-1} P(\Lambda_{ij}|q)$, the algorithm proceeds in two steps. First, a uniform variable $u_1 \in (0, 1)$ is chosen. If $u_1 < P(r_{ij} < \sigma)$, then simple rejection sampling can be used, wherein $\mathbf{\Lambda}_{ij}$ is sampled from the uniform distribution and rejected if the particles overlap. If $u_1 \geq P(r_{ij} < \sigma)$, then $\mathbf{\Lambda}_{ij}$ is chosen from the ITS method, for which the cumulative distribution function $\text{cdf}(\Lambda_{ij}) =$

$\int_0^{\Lambda_{ij}} P(\Lambda_{ij}|r_{ij}) d\Lambda_{ij}$ is calculated numerically, and a second random variable $u_2 \in (0, 1)$ is chosen such that $\text{cdf}^{-1}(u_2) = P(\Lambda_{ij})$. To obtain points uniformly distributed on the hypersphere, each is then multiplied by a unit vector randomly taken from a Gaussian distribution [75].

B. Gradient descent minimization

Instantaneous quenches of equilibrium configurations of soft spheres are evolved under a gradient descent (GD) algorithm. Particle motion is then overdamped, with a coefficient of static friction ζ such that

$$\zeta \dot{\mathbf{r}}_i = \mathbf{F}_i = -\frac{\partial U}{\partial \mathbf{r}_i}. \quad (4)$$

As such, \mathbf{F}_i/ζ has units of a velocity, and therefore

$$\Delta \mathbf{r}_i = \frac{\mathbf{F}_i}{\zeta} \Delta t. \quad (5)$$

The characteristic time Δt is chosen such that $\max(\Delta \mathbf{r}_i)$ remains below a certain threshold fraction Ξ of the diameter σ (or the maximum overlap in the system),

$$\Delta t = \frac{\zeta \Xi \sigma}{f_{\text{ub}}}, \quad (6)$$

where $f_{\text{ub}} = \max_i \|F_i\|$ is the maximum unbalanced force on a particle. The integral equation is then

$$\Delta \mathbf{r}_i = \frac{\Xi \sigma}{f_{\text{ub}}} \mathbf{F}_i. \quad (7)$$

To minimize the computational cost while closely approximating the exact GD minimization, we use an adaptive steepest descent algorithm, refashioned from that of Refs. [16,37]. The objective is to move slowly along the gradient direction, such that the gradient orientation only changes by a small fraction at each step. The time step Δt is therefore chosen initially by Eq. (6), but also follows the condition

$$\sum_i^N \frac{\mathbf{F}_i(t) \cdot \mathbf{F}_i(t + \Delta t)}{\|\mathbf{F}_i(t)\| \|\mathbf{F}_i(t + \Delta t)\|} = \cos \chi_{t,t+\Delta t} < 1 - \epsilon \quad (8)$$

with $0 < \epsilon \ll 1$. If the condition is violated, the step is rejected and attempted again with $\Xi \rightarrow \Xi/n$ for $n \in \mathbb{N}$. Special care must also be taken to leave particles in zero-energy kissing contact as required by the GD dynamics. Progressively smaller steps are therefore taken upon approaching each contact breaking event, until the dimensionless overlap between particles i and j is $-h_{ij} < 10^{-8}$. We note that while some contact breaking events are associated with rearrangements, not all of them are [76,77]. Particles are therefore allowed to oscillate in and out of contact without rearrangement. Lowering the minimum step size in contact breaking events increases the frequency with which these oscillations happen, leading to dramatic computational slowdowns without a noticeable effect on the relaxation times or the distribution of inherent states.

To further improve numerical efficiency, we employ a sticky algorithm which grows and shrinks the initial value of Ξ according to thresholding conditions. If n successive steps produce $\cos \chi_{t,t-1} < 1 - \epsilon$, then $\Xi \rightarrow n\Xi$, whereas if

n steps in a row produce a Ξ that must be decreased, then the initial guess of Ξ becomes $\Xi \rightarrow \Xi/n$. Empirically, we find that $\epsilon = 10^{-2}$ and $n = 5$ give stable results for the IS energy. Because the process is chaotic [39], changing n or ϵ changes an individual IS determination, but ensemble averages remain unaffected.

A configuration minimizes either to a jammed (UNSAT) or unjammed (SAT) state, as defined by the rigidity of its contact network after (recursively) removing rattlers [54,60–62]. Although in principle it is equally valid to determine if a state is jammed by its energy, pressure, or stress being nonzero, the numerical resolution of each of these quantities is far lower than for individual contacts. One should, however, note that during the GD minimization, several contacts are transient [37,40,78], and that a change to the contact network is not always associated with entering a new energetic sub-basin [76,77]. The jamming transition $\varphi_J(N)$ is then determined using several systems equilibrated at a given density and temperature. For each condition, the fraction of resulting jammed states is measured. For a fixed temperature, this fraction monotonically increases with φ , hence $\varphi_J(N)$ is naturally defined as the density for which half of all initializations jam. Empirically, an error function is found to capture well the growth of the fraction of jammed states with density, and is therefore used as a fitting form [79].

C. Effective potential hard sphere crunch

Hard sphere fluids are crunched following the effective potential approach (EP) of Ref. [47]. First, a regularization step (which is particularly important at low densities) reduces the smallest gap between particles to 1% of σ by adjusting the density accordingly. This scheme then alternatively iterates (i) an instantaneous expansion of particles, and (ii) a minimization of an effective potential via FIRE minimization [80] to open a (normalized) gap equivalent to the (normalized) gap of the previous iteration. The process continues until an isostatic structure is formed, as determined for gaps between contacts being no greater than $10^{-8}\sigma$. The choice of effective potential is taken to be a shifted and truncated logarithm of the gaps [81], which becomes the effective thermal potential for hard spheres near jamming [82,83]. In particular, we use $U = \sum_{ij} u(d_{ij})$, where $d_{ij} = -h_{ij}/d$ is the dimensionless overlap, with h_{ij} given by Eq. (2), and

$$u(d_{ij}) = \begin{cases} \infty, & d_{ij} < 0, \\ -\ln(d_{ij}) + \frac{1}{h_c}(1 + d_{ij}), & 0 < d_{ij} < h_c, \\ 0, & d_{ij} \geq h_c. \end{cases} \quad (9)$$

The cutoff h_c is set such that there is an average of $2d$ contacts per particle with $u(d_{ij}) > 0$. Two parameters are then adjusted to minimize the final jamming density: θ gives the expansion factor relative to the minimum gap in the system, and τ provides a cutoff on the minimization (and thus a cap on the effective thermalization) of the FIRE algorithm. Step (ii) terminates after τNd minimization steps if it cannot be completed. For standard HS, it was found that $\tau = 2$ and $\theta = 0.9$ were approximately optimal. In MK HS, the same parameters appear to be near optimal, in that they minimize the jamming density obtained, as illustrated in Fig. 1 for a typical example.

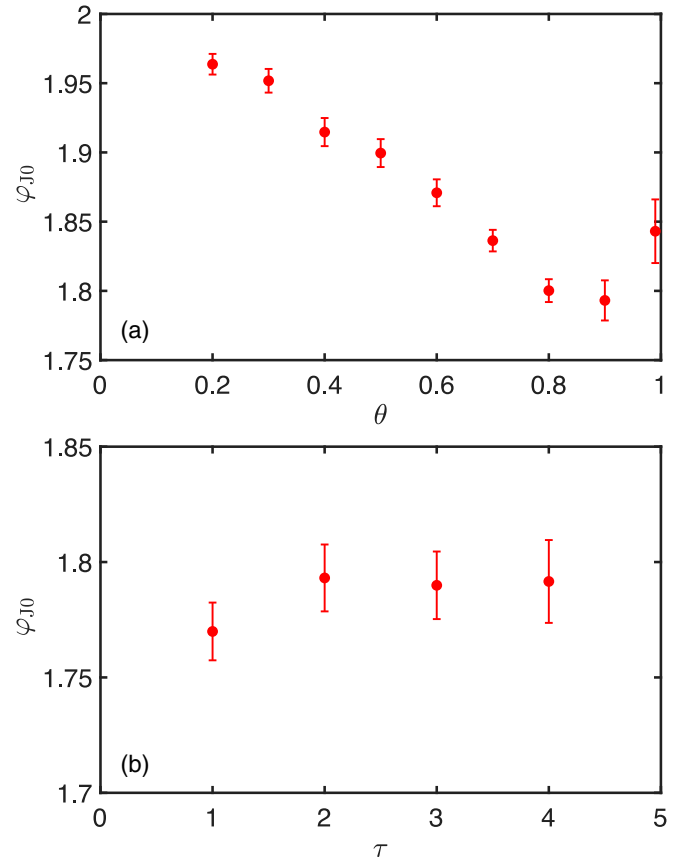


FIG. 1. The hard sphere crunching algorithm developed in Ref. [47] contains two optimization parameters, θ and τ , as described in Sec. III C. Optimal values yield the lowest jamming density φ_{J0} while not undergoing algorithmic arrest (leading to nonrigid packings). We show here parameter optimization for $N = 256$ particles in $d = 3$ with an initial liquid density $\varphi_{\text{eq}} = 0.5 \ll \varphi_{\text{on}}$, well below the onset. (a) Using a fixed value of the cutoff $\tau = 2$, the optimal expansion factor minimizes the function, $\theta \approx 0.9$. (b) Using a fixed $\theta = 0.9$, the value of φ_{J0} depends only weakly on τ . However, as for standard hard spheres [47], $\tau = 1$ corresponds to states that often lead to algorithmic arrest, and therefore they do not properly jam. We use the lowest integer value for which algorithmic arrest is avoided, $\tau = 2$.

D. Event-driven hard sphere crunch

Hard sphere fluids are also crunched using a modified version of an event-driven (ED) crunching algorithm developed by Lerner *et al.* to generalize the GD optimization scheme to systems with hard interactions [84]. However, unlike the affine field initially used to compress particles, here we isotropically grow particles. Although these processes are functionally similar, compression through an affine field requires manipulating the field to maintain periodic boundary conditions while isotropic growth presents no such difficulty. (Wherever possible, variable names here nevertheless follow those of Ref. [84].)

ED crunches require defining a velocity for each particle, an integration scheme, and a definition of the interparticle forces. For hard particles, forces only occur at kissing contact, which in practice means within a small numerical error, which here is $O(10^{-12}\sigma)$. By considering instantaneous changes in

distances between contacting particles i and j , with velocities V_i and V_j , respectively,

$$\begin{aligned} \dot{r}_{ij} &= \sum_k \frac{\partial r_{ij}}{\partial \vec{r}_k} \cdot \vec{V}_k \\ &= \sum_k (\delta_{jk} - \delta_{ik}) \vec{n}_{ij} \cdot \vec{V}_k = (\vec{V}_j - \vec{V}_i) \cdot \vec{n}_{ij}, \end{aligned} \quad (10)$$

one can define the \mathcal{S} -matrix

$$\mathcal{S} = \frac{\partial r_{ij}}{\partial \vec{r}_k}. \quad (11)$$

The ket notation here encodes vectors, with capitalized letters denoting the $N \times d$ dimensional space of all particles, and lower-case letters denoting the N_c -dimensional space of contacts. From Eq. (11) one therefore obtains $|\dot{r}\rangle = \mathcal{S} |V\rangle$. In other words, the \mathcal{S} -matrix acts on the space of velocities to generate a space of contacts.

Through particle expansion at a rate $\dot{\gamma}$, contacting particles remain in kissing contact unless forced out by other particles, i.e.,

$$|\dot{r}\rangle = \mathcal{S} |V\rangle = |\dot{\sigma}\rangle = \dot{\gamma} |\sigma_0\rangle, \quad (12)$$

where $|\sigma_0\rangle$ is an N_c -element vector with all elements equal to the particle diameter at $t = 0$.

As in Ref. [84], we apply a simple (and standard) model for overdamped dynamics that involves embedding a system in a liquid and accounting for Stokes drag, $|F^{\text{drag}}\rangle = -\xi_0^{-1} |V\rangle$, while ignoring other hydrodynamic forces. The contact force between kissing contacts is then simply $|F^{\text{cont}}\rangle = \mathcal{S}^T |f\rangle$, where $|f\rangle$ encodes contact forces f_{ij} . Force balance dictates $|F^{\text{drag}}\rangle = -|F^{\text{cont}}\rangle$. Rearranging gives

$$|V\rangle = \xi_0 \mathcal{S}^T |f\rangle, \quad (13)$$

which can be put into the form of Eq. (12),

$$\mathcal{S} |V\rangle = \xi_0 \mathcal{S} \mathcal{S}^T |f\rangle = \dot{\gamma} |\sigma_0\rangle. \quad (14)$$

Defining $\mathcal{N} = \mathcal{S} \mathcal{S}^T$, which is invertible unless it is singular, we can then solve for the forces

$$|f\rangle = \xi_0^{-1} \dot{\gamma} \mathcal{N}^{-1} |\sigma_0\rangle. \quad (15)$$

Finally, inserting Eq. (15) into Eq. (13) yields the equation of motion

$$|V\rangle = \dot{\gamma} \mathcal{S}^T \mathcal{N}^{-1} |\sigma_0\rangle. \quad (16)$$

Integration then follows the explicit formulation of Ref. [84], which details how contact networks are defined and updated and how the process is iterated until a jammed configuration is reached. In particular, an isostatic structure is formed with gaps between contacts which are no greater than $10^{-8}\sigma$. The only difference here is that during each integration step every particle uniformly expands its diameter as $\sigma \rightarrow \sigma(1 + \dot{\gamma}\Delta t)$, which reduces the subsequent time to collision. For particles separated by $\Delta\vec{r}$ and time $t = 0$ with relative velocity $\Delta\vec{v}$, this time of collision is given by

$$\sigma^2 \left(1 + \frac{\sigma_0 \dot{\gamma} t}{\sigma}\right)^2 = (\Delta\vec{r} + t\Delta\vec{v})^2, \quad (17)$$

which can be rewritten as

$$(\Delta v^2 - \sigma_0^2 \dot{\gamma}^2) t^2 + 2(\Delta\vec{r} \cdot \Delta\vec{v} - \sigma \sigma_0 \dot{\gamma}) t + \Delta r^2 - \sigma^2 = 0. \quad (18)$$

The physical solution is then

$$t = \begin{cases} \frac{\Delta r^2 - \sigma^2}{2(\Delta\vec{r} \cdot \Delta\vec{v} - \sigma \sigma_0 \dot{\gamma})} & \text{if } |\Delta\vec{v}| = \sigma_0 \dot{\gamma}, \\ \frac{\sigma_0 \sigma \dot{\gamma} - \Delta\vec{r} \cdot \Delta\vec{v} - \sqrt{\kappa}}{\Delta v^2 - \sigma_0^2 \dot{\gamma}^2} & \text{otherwise,} \end{cases} \quad (19)$$

where

$$\kappa = (\Delta\vec{r} \cdot \Delta\vec{v})^2 - \Delta r^2 \Delta v^2 + (\sigma \Delta\vec{v} - \sigma_0 \dot{\gamma} \Delta\vec{r})^2. \quad (20)$$

As noted in Ref. [84], the natural choice of time units is $\dot{\gamma}^{-1}$ and force units is $\sigma_0 \dot{\gamma} / \xi_0$. What is often less appreciated is that throughout this scheme, numerical precision and the nonlinearity of the problem introduce gaps and overlaps between contacts, particularly over large integration times in Eq. (19). To mitigate these effects, the algorithm introduces two procedures, as detailed in the original work. First, the integration time t_{int} is taken in uniform intervals $t_{\text{int}} \dot{\gamma} = 10^{-4}$, until a collision takes place. Second, a gap correction procedure is taken periodically to either force the closure of accumulated gaps or to allow contacts to break. Taken together, these procedures allow the systematic control of allowed overlaps, which are taken to be numerically negligible (in our case, less than $10^{-12}\sigma$).

Note that the calculation of the equation of motion Eq. (16) involves inverting (or solving a matrix equation of) a sparse matrix of size $O(dN)$ at each step, the complexity of which generically scales as $O(d^2 N^2)$ using optimal solvers on generic sparse matrices. Additionally, the number of iterations scales as at least $O(dN)$, set by the number of contacts, though in practice this estimate is a drastic underestimation. The total simulation time therefore scales at least as $O(d^3 N^3)$. This limitation severely constrains the accessible size and dimension range for comparing with the previous two approaches and for extrapolating to the limit $d \rightarrow \infty$.

IV. THEORETICAL ANALYSIS

In this section, we describe the analytical estimates for the finite- d dynamical transition density and the replica symmetric (RS) jamming threshold density for hard spheres under the Gaussian cage approximation. These quantities help interpret and contextualize the numerical finite- d results, and their role in estimating $d \rightarrow \infty$ quantities. Note that to compare volume (and packing) fractions φ across dimensions, we correct for their asymptotic $d \rightarrow \infty$ scaling by considering $\widehat{\varphi} = 2^d \varphi / d$.

In this context, note that the mean-field $d \rightarrow \infty$ description leaves out perturbative corrections in the small parameter $1/d$ [8]. Because the MK model separates spatial structure from other dimensional effects, leaving only the latter, characteristic densities are expected to scale linearly with that parameter (see Table I),

$$\widehat{\varphi}_{\text{J0, on, th, d}}(d) = \widehat{\varphi}_{\text{J0, on, th, d}}^\infty - \tilde{a}/d + O(1/d^2), \quad (21)$$

where \tilde{a} is a constant, and the subscripts refer to the jamming, onset, threshold, and dynamical densities, respectively. Both $\widehat{\varphi}_{\text{J0, on, th, d}}^\infty$ and \tilde{a} should therefore be accessible through a linear fit from finite- d results.

TABLE I. Parameters for the fits to Eq. (21) for the $d \rightarrow \infty$ limit ($\widehat{\varphi}^\infty$) and the scaling prefactor with $1/d$ (\tilde{a}). RS and 1RSB calculations of $\widehat{\varphi}^\infty$ are exact and are reported here with the highest published precision [22,87]; finite- d corrections to the 1RSB calculation have not been computed; all other quantities are fitted to data, with parentheses giving the 95% confidence interval.

Quantity	RS/1RSB	$\widehat{\varphi}^\infty$	\tilde{a}
$\widehat{\varphi}_d$	RS	4.8067...	0.440(3)
$\widehat{\varphi}_{th}$	RS	6.2581...	2.467(1)
$\widehat{\varphi}_{th}$	1RSB	6.86984...	

A. Dynamical transition density

A finite-dimensional estimate of the mean-field dynamical transition for MK systems can be obtained under the Gaussian cage approximation as [22,57,85]

$$\begin{aligned} \frac{1}{\widehat{\varphi}_d} &= -\max_A \frac{2A}{V_d \sigma^d} \frac{\partial}{\partial A} \int q_{A/2}(\mathbf{r}) \log q_{A/2}(\mathbf{r}) d\mathbf{r} \\ &= -\max_A 2dA \frac{\partial}{\partial A} \int_0^\infty r^{d-1} q_{A/2}(r/\sigma) \log q_{A/2}(r/\sigma) dr, \end{aligned} \quad (22)$$

where

$$q_{A/2}(r) = \int_0^\infty dy e^{-\beta u(y)} \left(\frac{y}{r}\right)^{\frac{d-1}{2}} e^{-\frac{(r-y)^2}{2A}} \frac{\sqrt{ry}}{A} I_{\frac{d-2}{2}}\left(\frac{ry}{A}\right), \quad (23)$$

$u(y)$ is the interparticle potential as a function of the interparticle distance y , and $I_n(x)$ is the modified Bessel function. This expression can be evaluated numerically for any d , u , and β .

For hard spheres, the potential is infinite for $0 \leq y < \sigma$ and zero for $y \geq \sigma$, thus resulting in the lower limit of Eq. (23) becoming σ and $\exp[-\beta u(y)] \rightarrow 1$. The resulting deviation of $\widehat{\varphi}_d$ from the $d \rightarrow \infty$ hard sphere result is remarkably small, even in $d = 2$. Considering higher-order corrections to Eq. (21) gives $\widehat{\varphi}_d = \widehat{\varphi}_d^\infty - \tilde{a}_1/d + \tilde{a}_2/d^2 + \tilde{a}_3/d^3$, where $\widehat{\varphi}_d^\infty = 4.8067, \dots$, $\tilde{a}_1 = 0.440(3)$, $\tilde{a}_2 = 0.38(2)$, and $\tilde{a}_3 = 0.91(4)$. Although non-Gaussian corrections are expected to be sizable [86], thus possibly affecting the estimate of $\widehat{\varphi}_d$, numerical results generally agree with this prediction [69].

In harmonic systems, we instead analyze the dynamical temperature, T_d , which can be obtained by numerically solving for the function $\widehat{\varphi}_d(T)$, and inverting to yield $T_d(\widehat{\varphi})$. Finite- d corrections are similarly small.

B. Finite-dimensional jamming threshold

Using the same Gaussian-cage approximation, it is also possible to estimate the finite- d correction to the RS threshold density, which has long been interpreted as the density at which jammed states appear in sufficient number for a finite complexity to be computed (see Refs. [8,67] and Ref. [22], Sec. 7.4.3). It should be noted that the RS threshold is merely an approximation of the proper $d \rightarrow \infty$ threshold, which significantly overshoots both the RLG and MK jamming transitions, thus calling into question the applicability of such calculations to this problem (see Ref. [40] for a thorough

discussion). Nevertheless, its dimensional scaling here provides some insight into the magnitude of finite- d corrections for similar quantities.

Specifically, the approximation gives [22,55]

$$\frac{1}{\widehat{\varphi}_{th}} = \max_A \frac{d}{4A} \int_0^1 r^{d-1} (r-1)^2 e^{-\frac{(r-1)^2}{4A}} dr, \quad (24)$$

which can also be numerically evaluated for any d . Fitting the asymptotic behavior, for $d \geq 5$, we find $\tilde{a} = 2.467(1)$, which is nearly an order of magnitude larger than for $\widehat{\varphi}_d$.

Because the RS threshold is unstable to further breaking of the replica symmetry, a one-step replica symmetry breaking (1RSB) estimate for $d \rightarrow \infty$ has also been obtained, $\widehat{\varphi}_{th}^{1RSB} = 6.86984 \dots$ [87]. Although this 1RSB threshold is itself unstable, higher-order replica symmetry breaking corrections are assumed—by analogy to what is observed in certain spin glass models [88]—to only lightly affect its numerical value. (In any case, these corrections would only increase the resulting density.) We thus consider here $\widehat{\varphi}_{th}^{1RSB}$ to be a reasonable approximation of $\widehat{\varphi}_{th}^{\text{fullRSB}}$. Because computing $1/d$ corrections to this approximation is quite involved, however, these are left for future analysis.

V. RESULTS AND DISCUSSION

The numerical results for relaxation, crunching, and IS memory in MK systems obtained as described in Sec. III are compared here with the analytical results from Sec. IV and the RLG results of Ref. [40].

A. Relaxation dynamics

We first consider GD dynamics of MK soft spheres, starting from an infinite-temperature configuration with purely random initial particle positions. By examining the relaxation, aging, and the unstressed (SAT) or frustrated (UNSAT) nature of the final state, we seek to validate comparable observations for the RLG [40]. We specifically compare and contrast the behavior of the two models far below ($\widehat{\varphi}_{MK} = 2$) and far above ($\widehat{\varphi}_{MK} = 6$) jamming, after rescaling density, mean-squared displacement Δ (MSD), and characteristic timescale as [40]

$$t_{MK} = 2t_{RLG}, \quad \Delta_{MK} = \frac{1}{2}\Delta_{RLG}, \quad \widehat{\varphi}_{MK} = 2\widehat{\varphi}_{RLG}, \quad (25)$$

such that the two models should coincide in the $d \rightarrow \infty$ limit. We otherwise follow the definitions of Ref. [40] for the various observables. For times to remain finite in the limit $d \rightarrow \infty$, and thus comparable across d , the friction coefficient is scaled as

$$\widehat{\zeta} = \frac{\sigma^2}{2d^2} \zeta, \quad (26)$$

which then sets the characteristic time in Eq. (6). The MSD is further made unitless and scaled with a factor of d to ensure a finite value as $d \rightarrow \infty$, such that

$$\widehat{\Delta}(t, t') = \frac{d}{N\sigma^2} \sum_i \langle [\mathbf{r}_i(t) - \mathbf{r}_i(t')]^2 \rangle. \quad (27)$$

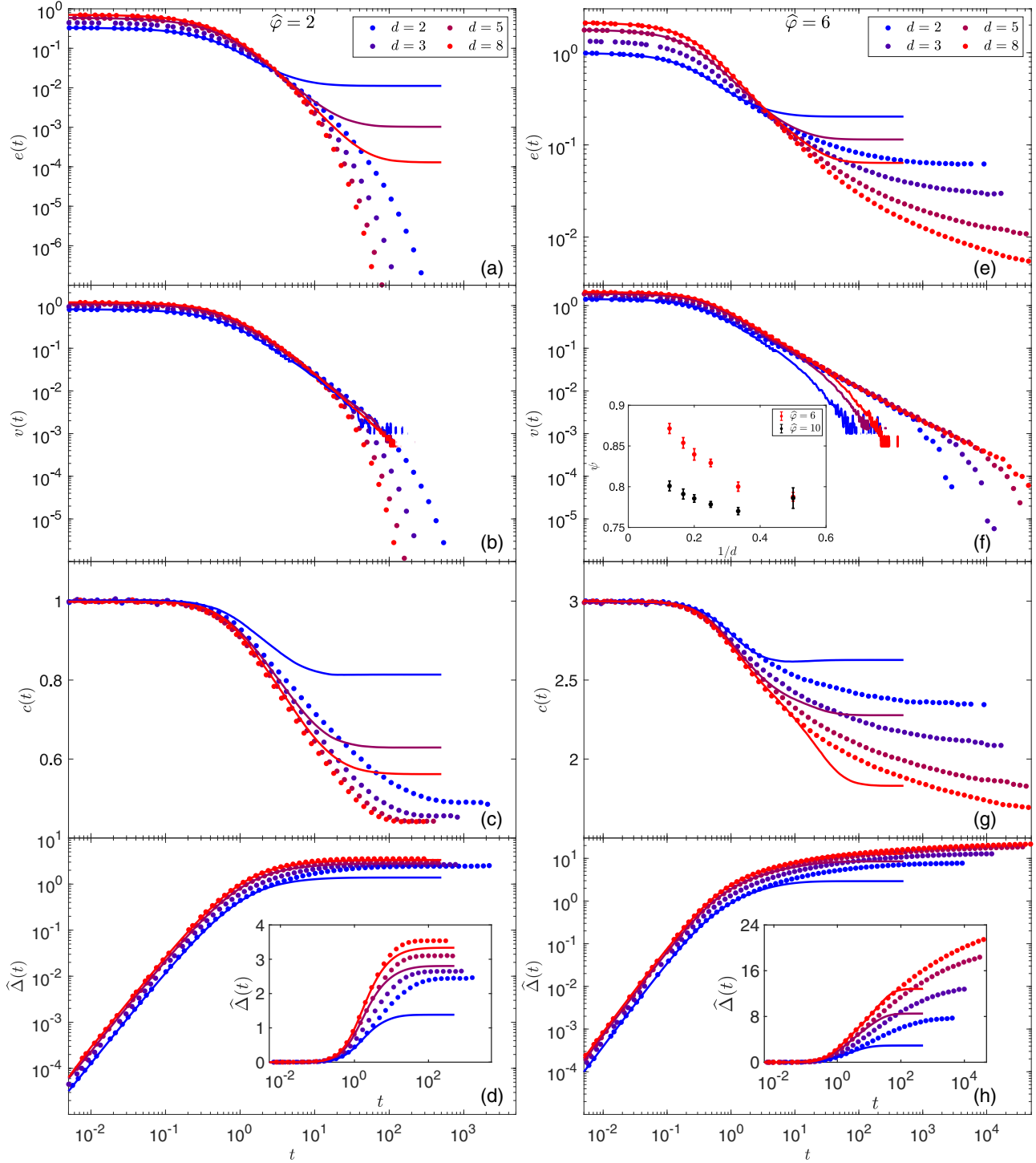


FIG. 2. Relaxation dynamics across dimension both (a)–(d) below jamming (at $\hat{\varphi} = 2$) and (e)–(h) above jamming (at $\hat{\varphi} = 6$) of the energy per particle (a),(e) $e(t)$, (b), (f) velocity $v(t)$, (c),(g) isostaticity index (or scaled contact number) $c(t)$, and (d),(h) rescaled MSD $\hat{\Delta}(t)$. The MK results (points) in $d = 2, 3, 5,$ and 8 are compared with RLG results (lines) in $d = 2, 5,$ and 8 taken from Ref. [40] [after rescaling to make the two DMFT descriptions equivalent, as in Eq. (25)]. The inset in (f) shows the power-law scaling behavior given by Eq. (31) as a function of d for two densities above jamming, $\hat{\varphi} = 6$ and 10 . The insets in (d) and (h) show log-lin plots of the main panel data.

(The hatted quantity distinguishes the rescaled MSD from the standard MSD, but directly corresponds to that measured in Ref. [40].) The isostaticity index (or scaled contact number) $c(t)$ is meanwhile the number of contacts per particle divided

by the number at isostaticity, $2d$,

$$c(t) = \frac{1}{2dN} \sum_{ij} \Theta(-h_{ij}(t)), \quad (28)$$

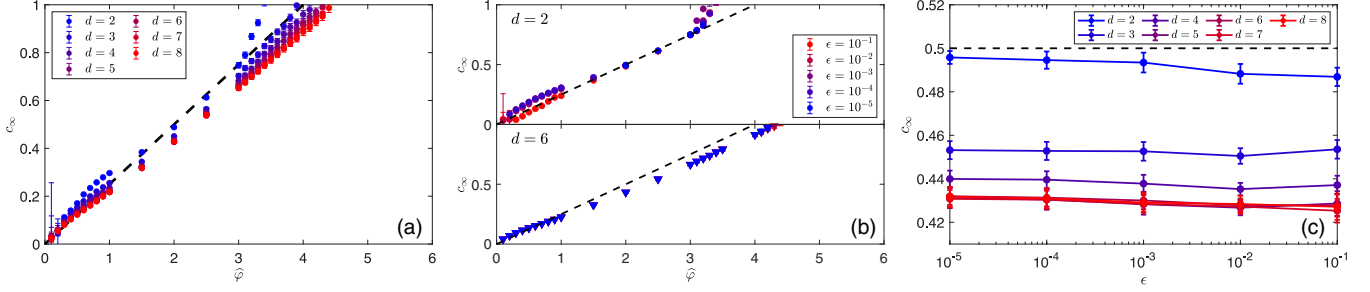


FIG. 3. (a) Final contact number, c_∞ , in systems below jamming for various d and $\hat{\varphi}$ for $\epsilon = 10^{-2}$. The low-density asymptotic prediction $c_\infty \approx \hat{\varphi}_{\text{MK}}/4$ (dashed black line) is approached as $d \rightarrow \infty$. (b) Same quantity in $d = 2$ and 6 for several ϵ , demonstrating that c_∞ rapidly converges at all densities for $\epsilon < 10^{-1}$ in $d = 2$ and for $\epsilon \leq 10^{-1}$ in $d = 6$. (c) At $\hat{\varphi} = 2$, c_∞ shows a much stronger dependence on d than on ϵ .

the per-particle energy is simply scaled as

$$e(t) = \frac{\epsilon}{2dN} \sum_{ij} h_{ij}^2(t) \Theta(-h_{ij}(t)), \quad (29)$$

and the velocity follows as

$$v(t) = \sqrt{-\frac{\partial e(t)}{\partial t}}. \quad (30)$$

That said, because the MK and RLG models present distinct numerical and theoretical challenges in finite d , features that robustly appear in both almost surely also appear in the DMFT.

Figure 2 shows that the initial time relaxation of the MK and RLG models is essentially equivalent in all d , both below and above jamming. This correspondence reflects the single-particle nature of optimization at very short times. For $t \geq 1$, the many-body nature of the MK model results in quantitative dynamical differences, but as d increases, this difference seemingly vanishes as well. In particular, for both models the average energy per particle e and the average velocity $v = \langle |\mathbf{v}(t)| \rangle$ decay exponentially below and algebraically above jamming [39,40],

$$v(t) \sim t^{-\psi}, \quad e(t) - e_\infty \sim t^{-(2\psi-1)}, \quad (31)$$

where $e_\infty = \lim_{t \rightarrow \infty} e(t)$. We find that the weak dimensional dependence of ψ for two such densities [Fig. 2(f), inset] is numerically consistent with previous reports for RLG [40] and $d = 3$ inverse-power MK models [39]. Furthermore, only minor deviations are observed in a variety of standard non-MK interparticle potentials (including both $d = 2$ and 3 Kob-Andersen Lennard-Jones and inverse-power potentials and $d = 2-4$ and 8 harmonic potentials) [39]. This relaxation behavior should therefore be considered to be a robust feature of the DMFT.

The MSD of the MK model likewise converges to that of the RLG as $d \rightarrow \infty$. Below jamming, Δ quickly plateaus as a stable unjammed state is reached. Above jamming, by contrast, the MSD continuously drifts upward. This drifting regime coincides with the algebraic decay of the energy and velocity, thus indicating that the system reaches ever lower energy states. While the drift is partially obscured in the low- d RLG, in the MK model the (sublogarithmic) growth is clearly visible even in $d = 2$ [see Fig. 2(h), inset]. We therefore

confirm that whether a liquid jams or not following GD minimization results in two drastically different behaviors. The former does so exponentially quickly; the latter slowly finds ever lower energy states in a process of athermal aging, as previously reported in Refs. [38–40,89,90]. Within a context of finite-precision calculations, the optimization process is necessarily truncated (e.g., once the gradient falls below a given threshold). This robustly universal scenario therefore challenges the traditional assumption that jammed states obtained by simple minimization are purely static [79]. This effect, while never reported in non-MK systems, is nevertheless expected to affect generic soft sphere systems, as evidenced by the power-law behavior of the velocity in Ref. [39]. Confirmation of this effect, however, is left for future work.

A key discrepancy between the RLG and MK results is observed in the average contact number at long times, c_∞ . In both systems, low-density states are expected to approach $c_\infty \equiv \lim_{t \rightarrow \infty} c(t) \approx \hat{\varphi}_{\text{MK}}/4$ in the joint dilute, $\hat{\varphi} \ll \hat{\varphi}_{\text{J0}}$, and high-dimensional limits [40]. In the RLG, this relationship holds until $\hat{\varphi}_{\text{RLG}} \approx 1.25$ ($\hat{\varphi}_{\text{MK}} \approx 2.5$), and is therefore captured in Fig. 2(c), for which $\hat{\varphi}_{\text{RLG}} = 1$. The curves, however, differ significantly, with $c_\infty^{\text{RLG}} \rightarrow 0.5$ and $c_\infty^{\text{MK}} \rightarrow 0.425$. (See Ref. [40] for higher-dimensional data and a discussion of the $d \rightarrow \infty$ limit.) To make sense of this difference, we consider two possible sources of discrepancy: the density and ϵ dependence of c_∞^{MK} .

For $\hat{\varphi}_{\text{MK}} \leq 0.5$, the relationship $c_\infty \approx \hat{\varphi}_{\text{MK}}/4$ appears to hold as $d \rightarrow \infty$ [Fig. 3(a)], in agreement with the analytical result for asymptotically low densities. However, significant deviations develop beyond that point, which is far below where they emerge for the RLG. Could it be that the multibody nature of the MK model somehow reduces the quality of the minimization compared to the single-particle RLG model? It seems not. Decreasing the size of the smallest time step, ϵ , by orders of magnitude results in only minuscule quantitative changes compared to $\epsilon = 10^{-2}$ —the value used in the rest of this work. Figure 3(b) presents case studies in $d = 2$ and 6, and combined with Fig. 3(c), it shows that the effect only weakens as d increases. The difference between the MK and RLG contact numbers therefore persists in the slow minimization, $\epsilon \rightarrow 0$, and thermodynamic, $N \rightarrow \infty$, limits for any finite d . Given the theoretical expectation that the two should coincide in the $d \rightarrow \infty$ limit, this difference might be due to (stronger than expected) pre-asymptotic corrections

in the RLG, thus obfuscating the dimensional extrapolation. We note, in particular, that finite- d RLG minimizations below jamming do not systematically result in configurations with zero energy, unlike comparable MK minimizations.

Whatever the physical origin of this discrepancy may be, it has marked consequences on the extraction of $\widehat{\varphi}_{J0}$, which corresponds to $c_\infty = 1$ in these units. The pronounced deviation of the MK results from the low density scaling $c_\infty \approx \varphi_{MK}/4$ results in a higher jamming density than for the RLG, as can be qualitatively observed in Fig. 3. To quantitatively estimate $\widehat{\varphi}_{J0}$, in Sec. VB we follow the more computationally efficient approach described in Sec. IIIB using the fraction of systems jammed as a function of $\widehat{\varphi}$. The difference between the approaches here and there amounts to swapping the high-dimensional and thermodynamic limits, which is not expected to result in any numerical difference, as long as the fraction of rattlers, which decays exponentially quickly with dimension [33], is sufficiently small.

B. Hard and soft sphere jamming

To extract the thermodynamic lowest density jamming transition in a given dimension, $\widehat{\varphi}_{J0}(d, \infty)$, we use a scaling form (see Fig. 4)

$$\widehat{\varphi}_{J0}(d, \infty) - \widehat{\varphi}_{J0}(d, N) \sim 1/N \tag{32}$$

that satisfactorily describes the finite-size scaling for all d and all algorithms considered. Equation (32), interestingly contrasts strongly with the scaling form used for non-MK systems, $\widehat{\varphi}_{J0}(d, \infty) - \widehat{\varphi}_{J0}(d, N) \sim N^{-\nu/d}$ with $\nu \lesssim 1$ [47,79,91,92]. Such a difference is reminiscent of models with Ising criticality, for which the finite-size scaling of the critical temperature has $\alpha = \tilde{\nu}d$ for constant $\tilde{\nu}$ below the upper critical dimension and $\alpha = 2$ above the upper critical dimension [93,94]. However, given that the upper critical dimension for jamming has been argued to be $d_u = 2$ [33,35,64], one might have expected finite-size corrections for both MK and non-MK models to scale similarly in $d > 2$. It is unclear why they do not, though one possibility is that strong preasymptotic corrections somehow associated with the complex structure of hard sphere fluids (relative to the minimally structured MK model) might obfuscate the proper critical scaling (see Table II).

In all three cases, the dimensional scaling appears to follow Eq. (21) [see Fig. 4(d) and Table III], with a roughly similar dimensional prefactor. Just like for the Gaussian cage approximation discussed in Sec. IVA, that scaling prefactor is about an order of magnitude larger than for $\widehat{\varphi}_d$. The (lack of) dimensional dependence in $\widehat{\varphi}_d$ might therefore reflect a cancellation of terms in Eq. (22). (The physical origin of that cancellation, however, is not obvious at this point.) More significantly, all three estimates for $\widehat{\varphi}_{J0}(d \rightarrow \infty)$ are much lower than $\widehat{\varphi}_{th}$, thus confirming the distinctness of that theoretical quantity from actual jamming densities.

The numerical results for the different algorithms, however, are not consistent with each other. In particular, the EP scheme gives much larger jamming densities than soft

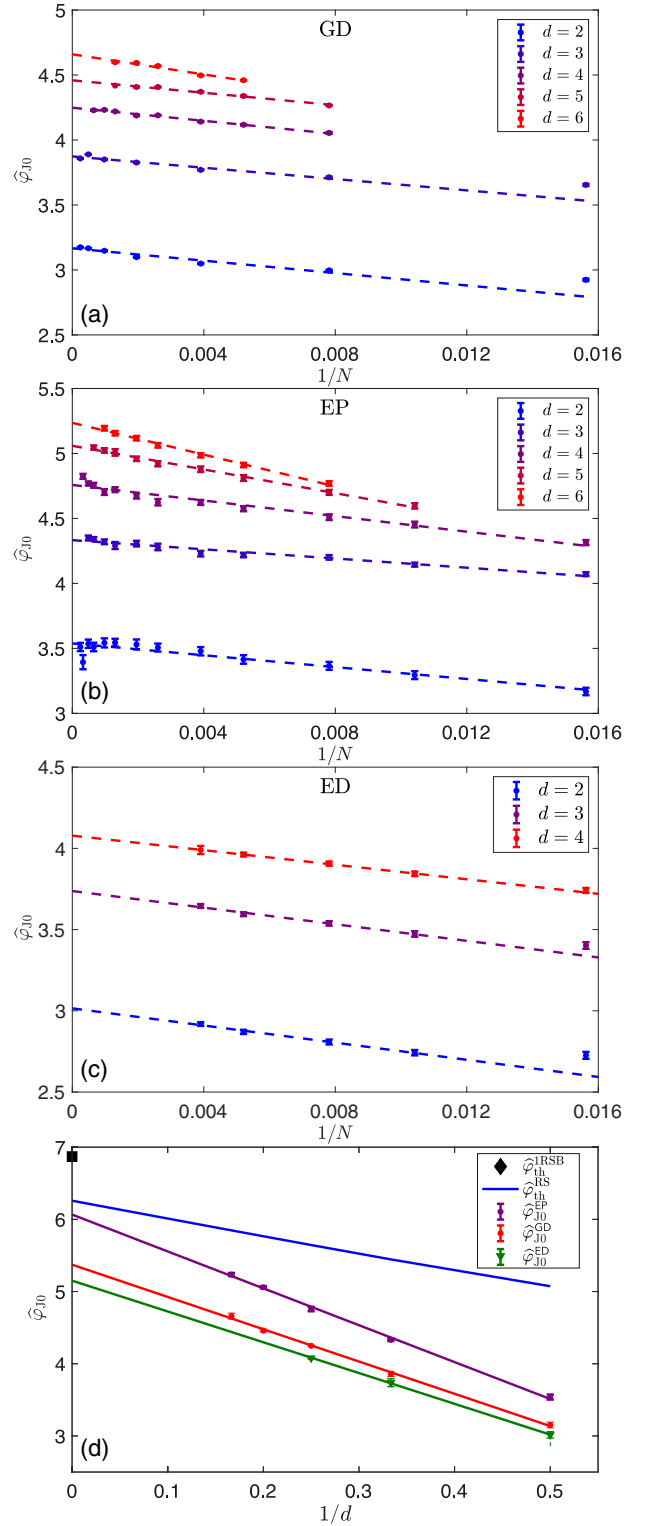


FIG. 4. Finite-size scaling of the jamming transition using (a) gradient descent (GD) minimization as well as (b) effective potential (EP) and (c) event-driven (ED) crunches. For each, linear fits to Eq. (32) are given. (d) Comparison of the $N \rightarrow \infty$ jamming transition and threshold densities in MK systems with linear fits to Eq. (21); see Table III for parameters.

TABLE II. Comparison of φ_{j0} in MK systems. Extrapolations to the limit $N \rightarrow \infty$ are made using Eq. (32) with maximum N reported. All values of φ_{j0} are found through finite-size scaling using D_d boundary conditions [56,71].

d	φ_{j0}	$\widehat{\varphi}_{j0}$	max N	Method
2	1.51(2)	3.02(4)	256	ED
	1.583(16)	3.17(3)	4096	SS
	1.769(18)	3.54(4)	4096	EP
3	1.40(2)	3.74(5)	256	ED
	1.453(10)	3.87(3)	4096	SS
	1.625(7)	4.333(19)	2048	EP
4	1.020(4)	4.079(14)	256	ED
	1.062(3)	4.249(11)	1536	SS
	1.189(8)	4.76(3)	3072	EP
5	0.697(3)	4.46(2)	768	SS
	0.790(3)	5.059(16)	1536	EP
6	0.437(4)	4.66(4)	768	SS
	0.491(2)	5.24(2)	1024	EP

sphere GD and hard sphere ED. The difference might be due to EP minimization permitting some degree of (effective) thermalization compared to the other two. The minimization step of EP indeed explicitly uses an effective thermal potential to open up a gap large enough for the expansion step to take place. As further support for this interpretation, we note that a previous soft sphere estimate obtained using a (FIRE) minimizer—known for having a higher degree of thermalization than GD—resulted in even denser jammed states [22]. Whatever the physical origin of this effect, it is much more pronounced in MK than in non-MK models [95] (see also Ref. [66]). This marked difference likely reflects the lack of a well-defined liquid shell structure to accompany caging in MK models, thus expanding the number of possible relaxation pathways. Although this effect has not yet been systematically studied—and is left as future work—this analysis already makes it clear that the EP scheme is generally ill-suited for identifying low-density jammed states. (The recently described CALiPPSO scheme is expected to fare even worse by this measure, given its built-in reliance on thermalization [61].)

TABLE III. Summary of the $d \rightarrow \infty$ limit of $\widehat{\varphi}_{j0}$ as extracted from results from GD minimization of the RLG, GD, and FIRE minimization of the MK, as well as the effective potential (EP) and event-driven (ED) hard sphere crunches.

$\widehat{\varphi}_{j0}$	\tilde{a}	System	Minimizer	Ref.
4.2(1)		RLG	GD	[40]
5.8		MK	FIRE	[22] (Fig. 9.2)
5.37(10)	4.5(3)	MK	GD	this work
6.08(14)	5.3(5)	MK	EP	this work
5.1(3)	4.3(7)	MK	ED	this work

One might posit that the difference between HS crunches and SS minimization originates from hard and soft spheres experiencing significantly different landscapes, with some of the barriers in the former turning into mere saddles in the latter, for example. The ED crunching scheme results support this interpretation, albeit only marginally. In low d , ED—the GD analog for HS—reaches jamming at slightly lower densities than actual GD for SS. The extrapolation error, however, is too large to discern whether the effect is systematic or not in the limit $d \rightarrow \infty$. In any event, this near coincidence between two markedly different algorithms (see Sec. VA) suggests that the $d \rightarrow \infty$ jamming density estimate they provide might be closer to the relevant DMFT prediction than that obtained from the RLG model. To compare jamming density results with the RLG and DMFT analysis, the lowest jamming density achieved using the different schemes is also considered. For soft spheres, configurations are first equilibrated at $T = \infty$, which corresponds to the canonical quench of Refs. [40,54,79]. For hard spheres, all liquid configurations equilibrated below an onset density $\widehat{\varphi}_{\text{on}}$ crunch towards the same (lowest) jamming density.

C. Inherent state memory

Section VB considered infinite temperature quenches for soft spheres and low density crunches for hard spheres, aiming to achieve low-density jammed systems. We now consider the impact of changing the equilibration temperature and density, respectively, on IS determination.

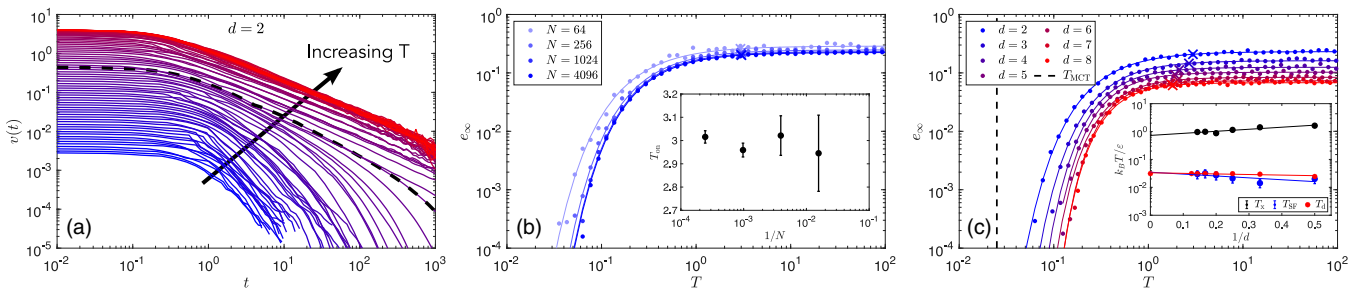


FIG. 5. (a) Velocity evolution of $d = 2$ soft spheres undergoing a GD minimization from configurations initially equilibrated at $T = 10^{-3}$ – 10^2 . The change from exponential to algebraic decay is fairly sharp (dashed line), thus identifying T_{SF} . (b) The inherent state energy for $d = 2$ over the same temperature is found to vary only weakly with system size. Inset: The crossover T_x (crosses), as defined in the text, is similarly only weakly d -dependent. (c) The inherent state energy in $d = 2$ – 8 presents a smooth d dependence. Inset: The weak dimensional trends of both T_x and T_{SF} are consistent with $T_{\text{SF}} \leq T_d < T_x$. As a guide to the eye, in (b) and (c) the inherent state energy is phenomenologically described as $\log e_\infty = a - bT^{-c}$, where a , b , and c are fit parameters.

By analogy with abstract models of spin glasses, the GD minimization of soft spheres is expected to exhibit two characteristic temperatures: a state following temperature T_{SF} and an onset temperature T_{on} , with $T_{\text{SF}} < T_d < T_{\text{on}}$ [17]. The first separates two relaxation regimes. For $T \geq T_{\text{SF}}$, the relaxation to the nearest minimum follows a nontrivial power law, whereas for $T < T_{\text{SF}}$, the relaxation to the nearest minimum is exponentially fast. The second is such that systems equilibrated at $T > T_{\text{on}}$ (or $\widehat{\varphi}_{\text{eq}} < \widehat{\varphi}_{\text{on}}$) minimize to a statistically similar set of inherent states, whereas those equilibrated at $T < T_{\text{on}}$ (or $\widehat{\varphi}_{\text{eq}} > \widehat{\varphi}_{\text{on}}$) result in IS that depend on T [3,48–51] (or $\widehat{\varphi}_{\text{eq}}$ [43–47]). For crunching algorithms, a similar onset density is expected, but the routines do not naturally lend themselves to state-following analyses.

Results for the GD minimization of soft spheres for $d = 2$ –8 are presented in Fig. 5. The systematic study of $d = 2$ systems suggests that finite-size effects are fairly weak. Relatively small system sizes, $N = 1024$ for $d = 2$ –5 and $N = 2048$ for $d = 6$ –8 [Fig. 5(c)], are therefore considered. Strictly speaking, however, the value of T_{SF} extracted is an upper bound, as finite-size systems give rise to an exponential cutoff to an otherwise (expected) power-law decay. The velocity decay results scale similarly in all dimensions, thus allowing T_{SF} to be straightforwardly extracted [Fig. 5(c), inset]. This dimensional trend validates the robustness of the power-law relaxation regime previously reported for a wide variety of glass formers—including $d = 3$ MK [38,39]. The effect should therefore persist in the $d \rightarrow \infty$ limit, and thus be described by the DMFT.

The onset temperature is more problematic. Because the IS energy varies for all T , no temperature cleanly separates a T -independent regime in any finite d . In soft spheres, the onset is therefore seemingly not a true transition, in agreement with recent results from spin glass models which strongly suggest that $T_{\text{on}} = \infty$ [17,41]. To characterize the dimensional evolution of inherent state energy, we nevertheless define a crossover temperature such that $e(T_x) = fe_\infty$ with arbitrary parameter f . Here, we choose $f = 0.9$, but the dimensional trend is robust to even fairly large changes to f . Empirically, we find that the logarithm of the resulting characteristic temperatures scale linearly with $1/d$,

$$\log T(d) = \log T^\infty + \tilde{b}/d, \quad (33)$$

with $T_x^\infty = 0.73(18)$ with $\tilde{b} = 1.7(9)$ and $T_{\text{SF}}^\infty = 0.035(17)$ with $\tilde{b} = -2(2)$. Using the results for T_d from Sec. IV A, we therefore confirm that $T_{\text{SF}} \leq T_d < T_x$ as expected, though we cannot conclude whether T_{SF} and T_d are distinct or not in the $d \rightarrow \infty$ limit. If a difference does persist in the DMFT, however, it is likely quite small.

The HS crunching algorithms are more consistent with the presence of a nontrivial onset, although $\widehat{\varphi}_{\text{on}} = 0$ cannot be excluded either (see Fig. 6). The IS density indeed seemingly follows the same empirical form as standard HS [47],

$$\widehat{\varphi}_i(\widehat{\varphi}_{\text{eq}}) = \widehat{\varphi}_{\text{J0}} + ab \log\{1 + \exp[(\widehat{\varphi}_{\text{eq}} - \widehat{\varphi}_{\text{on}})/b]\}, \quad (34)$$

where $\widehat{\varphi}_{\text{J0}}$ is the lowest jamming density quoted in Sec. V B, and a and b are fit parameters. Following Eq. (32) (and noting only a light system size dependence), we can extract a thermodynamic estimate of $\widehat{\varphi}_{\text{on}}$ for each d [Fig. 6(b)] on the

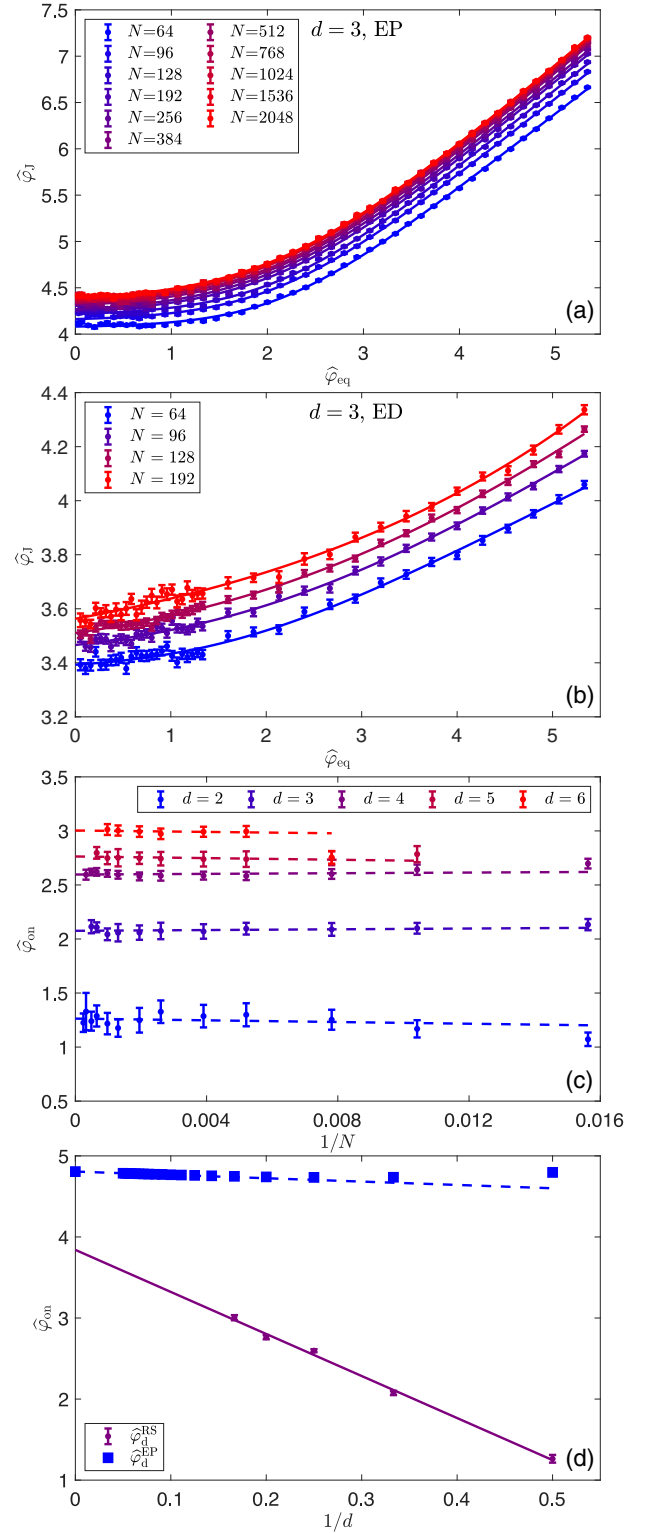


FIG. 6. (a) EP and (b) ED crunching exhibit strong signatures of inherent state memory, wherein $\widehat{\varphi}_i$ is a function of the initial equilibrated density $\widehat{\varphi}_{\text{eq}}$. Data are shown here for a variety of system sizes in $d = 3$, fitted to Eq. (34) (solid lines). (c) From the fit in (a), the onset density $\widehat{\varphi}_{\text{on}}$ is found to have only a weak N dependence. The value extracted for $\widehat{\varphi}_{\text{J0}}$ is shown in Fig. 4(d). (d) Comparison of the hard sphere MK dynamical transition from Eq. (22) and the onset density for the EP protocol from Eq. (34). Linear fits to Eq. (21) (lines) suggest that the two remain distinct as $d \rightarrow \infty$.

EP data. The resulting estimate is well described by Eq. (21) [Fig. 6(d)], thus yielding $\widehat{\varphi}_{\text{on}}^{\infty} = 3.84(18)$ with $\tilde{a} = 5.2(6)$. As expected, this value is well below $\widehat{\varphi}_d$ (see Sec. IV A) as for standard hard spheres. The scaling form used, however, is equally compatible with $\widehat{\varphi}_{\text{on}}$ being a crossover, and therefore small deviations could well persist even in the low-density limit.

Because ED crunches are so computationally costly, we are here only able to demonstrate that $\widehat{\varphi}_{\text{on}}$ exists for small system sizes. This observation nevertheless confirms that an onset $\widehat{\varphi}_{\text{on}}$ is present in both crunching schemes considered here, thus complementing the fast compression results for $d = 3$ reported in Ref. [59]. We therefore expect the DMFT to predict such an onset, distinct from $\widehat{\varphi}_d$, be it trivial or not.

VI. CONCLUSION

The MK model presents a minimal spatial structure, thus making it ideal for anticipating the DMFT behavior through $d \rightarrow \infty$ extrapolations. In particular, its finite- d corrections to $\widehat{\varphi}_d$ and $\widehat{\varphi}_{10}$ are linear in $1/d$, as in Eq. (21), which contrast sharply with the highly nontrivial $1/d$ dependence of comparable quantities in standard hard spheres [56,66,95]. We have here found that the MK model also appears to have a distinct advantage over the RLG, in that the former exhibits finite-dimensional corrections that converge faster than the latter as $d \rightarrow \infty$. In addition to providing stronger quantitative estimates of $\widehat{\varphi}_{10}$, we have also found that the MK model is well suited to identify the onset and to differentiate it from the dynamical transition in all dimensions. Because as yet no sufficient solution to the out-of-equilibrium DMFT exists, and because the MK and RLG models are expected to converge in the $d \rightarrow \infty$ limit, it nevertheless behooves us to use whichever model is best suited to the DMFT quantity of interest, while understanding that the differences between these models may also provide a deeper physical understanding of the DMFT.

Several questions that target the notion of jamming more broadly also persist. First, both MK and RLG models exhibit a (sublogarithmic) continuous growth of the MSD (Sec. V A) upon GD quenches above jamming even in finite dimensions, thus calling into question the notion that jamming is purely static. Yet, to the best of our knowledge, this feature has not been reported in standard soft sphere models. Second, while the power-law relaxation of the velocity in systems prepared above jamming has been shown to be a generic landscape feature of glasses [39,40], the universality of the associated exponent has not been explained, nor has its clear dependence on $\widehat{\varphi} - \widehat{\varphi}_{10}$ in systems that exhibit jamming [Fig. 2(f), inset]. Third, while near optimal in nonshifted hard sphere models, the crunching algorithm via the log potential here far overshoots the jamming density found through soft sphere relaxation in all dimensions, making this approach clearly suboptimal. ED crunches fare far better in this respect, achieving a jamming density less than that of the soft sphere MK following gradient descent, albeit at a very steep computational cost. A clearer understanding of the algorithmic difficulty involved in identifying (low-density) jammed hard spheres through crunching might finally offer some well-needed insight into the classic experiments reporting *random close packing* densities in various systems [66].

ACKNOWLEDGMENTS

We thank Giampaolo Folena, Edan Lerner, Alessandro Manacorda, and Francesco Zamponi for useful discussions and the latter two also for sharing their RLG data. This work was supported by a grant from the Simons Foundation (Grant No. 454937). The simulations were performed at both Duke Compute Cluster (DCC)—for which the authors thank Tom Milledge’s assistance—and on Extreme Science and Engineering Discovery Environment (XSEDE), which is supported by National Science Foundation Grant No. ACI-1548562. Data relevant to this work have been archived and can be accessed at the Duke Digital Repository [96].

-
- [1] P. W. Anderson, Lectures on amorphous systems, in *Ill-Condensed Matter: Les Houches Session XXXI*, edited by R. Balian, G. Toulouse, and R. Maynard (North-Holland, Amsterdam, 1979), pp. 159–261.
 - [2] F. H. Stillinger, A Topographic View of Supercooled Liquids and Glass Formation, *Science* **267**, 1935 (1995).
 - [3] S. Sastry, P. G. Debenedetti, and F. H. Stillinger, Signatures of distinct dynamical regimes in the energy landscape of a glass-forming liquid, *Nature (London)* **393**, 554 (1998).
 - [4] P. G. Debenedetti and F. H. Stillinger, Supercooled liquids and the glass transition, *Nature (London)* **410**, 259 (2001).
 - [5] A. Altieri, F. Roy, C. Cammarota, and G. Biroli, Properties of equilibria and glassy phases of the random Lotka-Volterra model with demographic noise, *Phys. Rev. Lett.* **126**, 258301 (2021).
 - [6] A. Altieri and G. Biroli, Effects of intraspecific cooperative interactions in large ecosystems, *SciPost Phys.* **12**, 013 (2022).
 - [7] D. Facchetti, G. Biroli, J. Kurchan, and D. R. Reichman, Classical glasses, black holes, and strange quantum liquids, *Phys. Rev. B* **100**, 205108 (2019).
 - [8] G. Parisi and F. Zamponi, Mean-field theory of hard sphere glasses and jamming, *Rev. Mod. Phys.* **82**, 789 (2010).
 - [9] V. Ros, G. Ben Arous, G. Biroli, and C. Cammarota, Complex energy landscapes in spiked-tensor and simple glassy models: ruggedness, arrangements of local minima, and phase transitions, *Phys. Rev. X* **9**, 011003 (2019).
 - [10] G. Parisi, Infinite number of order parameters for spin-glasses, *Phys. Rev. Lett.* **43**, 1754 (1979).
 - [11] G. Parisi, A sequence of approximated solutions to the S-K model for spin glasses, *J. Phys. A* **13**, L115 (1980).
 - [12] D. Panchenko, The Parisi ultrametricity conjecture, *Ann. Math.* **177**, 383 (2013).
 - [13] T. R. Kirkpatrick and D. Thirumalai, Dynamics of the structural glass transition and the p-spin—interaction spin-glass model, *Phys. Rev. Lett.* **58**, 2091 (1987).

- [14] L. F. Cugliandolo and J. Kurchan, Analytical solution of the off-equilibrium dynamics of a long-range spin-glass model, *Phys. Rev. Lett.* **71**, 173 (1993).
- [15] M. Bernaschi, A. Billoire, A. Maiorano, G. Parisi, and F. Ricci-Tersenghi, Strong ergodicity breaking in aging of mean-field spin glasses, *Proc. Natl. Acad. Sci. USA* **117**, 17522 (2020).
- [16] G. Folena, S. Franz, and F. Ricci-Tersenghi, Gradient descent dynamics in the mixed p-spin spherical model: Finite-size simulations and comparison with mean-field integration, *J. Stat. Mech.* (2021) 033302.
- [17] G. Folena, S. Franz, and F. Ricci-Tersenghi, Rethinking mean-field glassy dynamics and its relation with the energy landscape: the surprising case of the spherical mixed p-spin model, *Phys. Rev. X* **10**, 031045 (2020).
- [18] V. Ros, G. Biroli, and C. Cammarota, Dynamical instantons and activated processes in mean-field glass models, *SciPost Phys.* **10**, 002 (2021).
- [19] T. Rizzo, Path integral approach unveils role of complex energy landscape for activated dynamics of glassy systems, *Phys. Rev. B* **104**, 094203 (2021).
- [20] G. Folena, G. Biroli, P. Charbonneau, Y. Hu, and F. Zamponi, Equilibrium fluctuations in mean-field disordered models, *Phys. Rev. E* **106**, 024605 (2022).
- [21] P. Charbonneau, J. Kurchan, G. Parisi, P. Urbani, and F. Zamponi, Glass and jamming transitions: From exact results to finite-dimensional descriptions, *Annu. Rev. Condens. Matter Phys.* **8**, 265 (2017).
- [22] G. Parisi, P. Urbani, and F. Zamponi, *Theory of Simple Glasses: Exact Solutions in Infinite Dimensions* (Cambridge University Press, Cambridge, 2020).
- [23] T. Maimbourg, J. Kurchan, and F. Zamponi, Solution of the dynamics of liquids in the large-dimensional limit, *Phys. Rev. Lett.* **116**, 015902 (2016).
- [24] G. Szamel, Simple theory for the dynamics of mean-field-like models of glass-forming fluids, *Phys. Rev. Lett.* **119**, 155502 (2017).
- [25] E. Agoritsas, G. Biroli, P. Urbani, and F. Zamponi, Out-of-equilibrium dynamical mean-field equations for the perceptron model, *J. Phys. A* **51**, 085002 (2018).
- [26] E. Agoritsas, T. Maimbourg, and F. Zamponi, Out-of-equilibrium dynamical equations of infinite-dimensional particle systems I. The isotropic case, *J. Phys. A* **52**, 144002 (2019).
- [27] E. Agoritsas, T. Maimbourg, and F. Zamponi, Out-of-equilibrium dynamical equations of infinite-dimensional particle systems. II. The anisotropic case under shear strain, *J. Phys. A* **52**, 334001 (2019).
- [28] E. Agoritsas, Mean-field dynamics of infinite-dimensional particle systems: Global shear versus random local forcing, *J. Stat. Mech.* (2021) 033501.
- [29] P. K. Morse, S. Roy, E. Agoritsas, E. Stanifer, E. I. Corwin, and M. L. Manning, A direct link between active matter and sheared granular systems, *Proc. Natl. Acad. Sci. USA* **118**, e2019909118 (2021).
- [30] A. Manacorda, G. Schehr, and F. Zamponi, Numerical solution of the dynamical mean field theory of infinite-dimensional equilibrium liquids, *J. Chem. Phys.* **152**, 164506 (2020).
- [31] M. Baity-Jesi and D. R. Reichman, On mean-field theories of dynamics in supercooled liquids, *J. Chem. Phys.* **151**, 084503 (2019).
- [32] T. Arnoux de Pirey, A. Manacorda, F. van Wijland, and F. Zamponi, Active matter in infinite dimensions: Fokker-Planck equation and dynamical mean-field theory at low density, *J. Chem. Phys.* **155**, 174106 (2021).
- [33] P. Charbonneau, E. I. Corwin, G. Parisi, and F. Zamponi, Jamming criticality revealed by removing localized buckling excitations, *Phys. Rev. Lett.* **114**, 125504 (2015).
- [34] S. Torquato and F. H. Stillinger, Jammed hard-particle packings: From Kepler to Bernal and beyond, *Rev. Mod. Phys.* **82**, 2633 (2010).
- [35] P. Charbonneau, E. I. Corwin, R. C. Dennis, R. Díaz Hernández Rojas, H. Ikeda, G. Parisi, and F. Ricci-Tersenghi, Finite-size effects in the microscopic critical properties of jammed configurations: A comprehensive study of the effects of different types of disorder, *Phys. Rev. E* **104**, 014102 (2021).
- [36] R. J. Speedy, Random jammed packings of hard discs and spheres, *J. Phys.: Condens. Matter* **10**, 4185 (1998).
- [37] E. Stanifer and M. Lisa Manning, Avalanche dynamics in sheared athermal particle packings occurs via localized bursts predicted by unstable linear response, *Soft Matter* **18**, 2394 (2022).
- [38] Y. Nishikawa, A. Ikeda, and L. Berthier, Relaxation dynamics of non-brownian spheres below jamming, *J. Stat. Phys.* **182**, 37 (2021).
- [39] Y. Nishikawa, M. Ozawa, A. Ikeda, P. Chaudhuri, and L. Berthier, Relaxation dynamics in the energy landscape of glass-forming liquids, *Phys. Rev. X* **12**, 021001 (2022).
- [40] A. Manacorda and F. Zamponi, Gradient descent dynamics and the jamming transition in infinite dimensions, *J. Phys. A* **55**, 334001 (2022).
- [41] G. Folena and F. Zamponi, On weak ergodicity breaking in mean-field spin glasses, *SciPost Phys.* **15**, 109 (2023).
- [42] S. Luding, So much for the jamming point, *Nat. Phys.* **12**, 531 (2016).
- [43] M. Ozawa, T. Kuroiwa, A. Ikeda, and K. Miyazaki, Jamming transition and inherent structures of hard spheres and disks, *Phys. Rev. Lett.* **109**, 205701 (2012).
- [44] L. Berthier, D. Coslovich, A. Ninarello, and M. Ozawa, Equilibrium sampling of hard spheres up to the jamming density and beyond, *Phys. Rev. Lett.* **116**, 238002 (2016).
- [45] M. Ozawa, L. Berthier, and D. Coslovich, Exploring the jamming transition over a wide range of critical densities, *SciPost Phys.* **3**, 027 (2017).
- [46] Y. Jin and H. Yoshino, A jamming plane of sphere packings, *Proc. Natl. Acad. Sci. USA* **118**, e2021794118 (2021).
- [47] P. Charbonneau and P. K. Morse, Memory formation in jammed hard spheres, *Phys. Rev. Lett.* **126**, 088001 (2021).
- [48] S. Sastry, Onset temperature of slow dynamics in glass forming liquids, *Phys. Chem. Commun.* **3**, 79 (2000).
- [49] S. Kamath, R. H. Colby, S. K. Kumar, and J. Baschnagel, Thermodynamic signature of the onset of caged dynamics in glass-forming liquids, *J. Chem. Phys.* **116**, 865 (2002).
- [50] Y. Brumer and D. R. Reichman, Mean-field theory, mode-coupling theory, and the onset temperature in supercooled liquids, *Phys. Rev. E* **69**, 041202 (2004).
- [51] S. Sastry, Glass-forming liquids and the glass transition: The energy landscape approach to dynamics and thermodynamics, *J. Indian I. Sci.* **86**, 731 (2006).

- [52] M. Skoge, A. Donev, F. H. Stillinger, and S. Torquato, Packing hyperspheres in high-dimensional Euclidean spaces, *Phys. Rev. E* **74**, 041127 (2006).
- [53] P. Charbonneau, A. Ikeda, G. Parisi, and F. Zamponi, Glass Transition and random close packing above three dimensions, *Phys. Rev. Lett.* **107**, 185702 (2011).
- [54] P. K. Morse and E. I. Corwin, Geometric signatures of jamming in the mechanical vacuum, *Phys. Rev. Lett.* **112**, 115701 (2014).
- [55] M. Mangeat and F. Zamponi, Quantitative approximation schemes for glasses, *Phys. Rev. E* **93**, 012609 (2016).
- [56] P. Charbonneau, Y. Hu, J. Kundu, and P. K. Morse, The dimensional evolution of structure and dynamics in hard sphere liquids, *J. Chem. Phys.* **156**, 134502 (2022).
- [57] G. Biroli, P. Charbonneau, Y. Hu, H. Ikeda, G. Szamel, and F. Zamponi, Mean-field caging in a random lorentz gas, *J. Phys. Chem. B* **125**, 6244 (2021).
- [58] G. Biroli, P. Charbonneau, E. I. Corwin, Y. Hu, H. Ikeda, G. Szamel, and F. Zamponi, Interplay between percolation and glassiness in the random Lorentz gas, *Phys. Rev. E* **103**, L030104 (2021).
- [59] R. Mari and J. Kurchan, Dynamical transition of glasses: From exact to approximate, *J. Chem. Phys.* **135**, 124504 (2011).
- [60] P. K. Morse and E. I. Corwin, Geometric order parameters derived from the Voronoi tessellation show signatures of the jamming transition, *Soft Matter* **12**, 1248 (2016).
- [61] C. Artiago, R. Díaz Hernández Rojas, G. Parisi, and F. Ricci-Tersenghi, Hard-sphere jamming through the lens of linear optimization, *Phys. Rev. E* **106**, 055310 (2022).
- [62] P. K. Morse and E. Corwin, Local stability of spheres via the convex hull and the radical Voronoi diagram, [arXiv:2309.16484](https://arxiv.org/abs/2309.16484).
- [63] M. van Hecke, Jamming of soft particles: Geometry, mechanics, scaling and isostaticity, *J. Phys.: Condens. Matter* **22**, 033101 (2010).
- [64] C. P. Goodrich, A. J. Liu, and S. R. Nagel, Finite-size scaling at the jamming transition, *Phys. Rev. Lett.* **109**, 095704 (2012).
- [65] F. H. Stillinger, *Energy Landscapes, Inherent Structures, and Condensed-Matter Phenomena* (Princeton University Press, Princeton, NJ, 2016).
- [66] P. K. Morse and P. Charbonneau, Amorphous packings of spheres, in *Packing Problems in Soft Matter Physics*, edited by H.-K. Chan, S. Hutzler, A. Mughal, C. S. O'Hern, Y. Wang, and D. Weaire (Royal Society of Chemistry, Cambridge, 2024).
- [67] R. Monasson, Structural glass transition and the entropy of the metastable states, *Phys. Rev. Lett.* **75**, 2847 (1995).
- [68] C. Rainone and P. Urbani, Following the evolution of glassy states under external perturbations: The full replica symmetry breaking solution, *J. Stat. Mech.* (2016) 053302.
- [69] P. Charbonneau, Y. Jin, G. Parisi, and F. Zamponi, Hopping and the Stokes–Einstein relation breakdown in simple glass formers, *Proc. Natl. Acad. Sci. USA* **111**, 15025 (2014).
- [70] C. Scalliet, L. Berthier, and F. Zamponi, Marginally stable phases in mean-field structural glasses, *Phys. Rev. E* **99**, 012107 (2019).
- [71] J. Conway and N. Sloane, Fast quantizing and decoding and algorithms for lattice quantizers and codes, *IEEE Trans. Inf. Theor.* **28**, 227 (1982).
- [72] For $d = 2$, the D_d boundary conditions reduce to that of Z_d , the standard square lattice.
- [73] Y. Nishikawa, A. Ikeda, and L. Berthier, Collective dynamics in a glass-former with Mari–Kurchan interactions, *J. Chem. Phys.* **156**, 244503 (2022).
- [74] L. Devroye, *Non-Uniform Random Variate Generation* (Springer, New York, 1986).
- [75] M. E. Muller, A note on a method for generating points uniformly on n-dimensional spheres, *Commun. ACM* **2**, 19 (1959).
- [76] P. Morse, S. Wijtmans, M. van Deen, M. van Hecke, and M. L. Manning, Differences in plasticity between hard and soft spheres, *Phys. Rev. Res.* **2**, 023179 (2020).
- [77] P. J. Tuckman, K. VanderWerf, Y. Yuan, S. Zhang, J. Zhang, M. D. Shattuck, and C. S. O'Hern, Contact network changes in ordered and disordered disk packings, *Soft Matter* **16**, 9443 (2020).
- [78] P. K. Morse, K. I. Alberto, J. D. Dietz, P. Charbonneau, and R. S. Hoy (unpublished).
- [79] C. S. O'Hern, L. E. Silbert, A. J. Liu, and S. R. Nagel, Jamming at zero temperature and zero applied stress: The epitome of disorder, *Phys. Rev. E* **68**, 011306 (2003).
- [80] E. Bitzek, P. Koskinen, F. Gähler, M. Moseler, and P. Gumbsch, Structural relaxation made simple, *Phys. Rev. Lett.* **97**, 170201 (2006).
- [81] F. Arceri and E. I. Corwin, Vibrational Properties of hard and soft spheres are unified at jamming, *Phys. Rev. Lett.* **124**, 238002 (2020).
- [82] C. Brito and M. Wyart, On the rigidity of a hard-sphere glass near random close packing, *Europhys. Lett.* **76**, 149 (2006).
- [83] A. Altieri, S. Franz, and G. Parisi, The jamming transition in high dimension: An analytical study of the TAP equations and the effective thermodynamic potential, *J. Stat. Mech.* (2016) 093301.
- [84] E. Lerner, G. Düring, and M. Wyart, Simulations of driven overdamped frictionless hard spheres, *Comput. Phys. Commun.* **184**, 628 (2013).
- [85] G. Biroli and P. Urbani, Liu–Nagel phase diagrams in infinite dimension, *SciPost Phys.* **4**, 020 (2018).
- [86] G. Biroli, P. Charbonneau, G. Folena, Y. Hu, and F. Zamponi, Local dynamical heterogeneity in simple glass formers, *Phys. Rev. Lett.* **128**, 175501 (2022).
- [87] P. Charbonneau, J. Kurchan, G. Parisi, P. Urbani, and F. Zamponi, Exact theory of dense amorphous hard spheres in high dimension. III. The full replica symmetry breaking solution, *J. Stat. Mech.* (2014) P10009.
- [88] T. Rizzo, Replica-symmetry-breaking transitions and off-equilibrium dynamics, *Phys. Rev. E* **88**, 032135 (2013).
- [89] P. Olsson, Relaxation times, rheology, and finite size effects for non-Brownian disks in two dimensions, *Phys. Rev. E* **105**, 034902 (2022).
- [90] J. T. Parley, R. Mandal, and P. Sollich, Mean-field description of aging linear response in athermal amorphous solids, *Phys. Rev. Mater.* **6**, 065601 (2022).
- [91] D. Vågberg, D. Valdez-Balderas, M. A. Moore, P. Olsson, and S. Teitel, Finite-size scaling at the jamming transition: Corrections to scaling and the correlation-length critical exponent, *Phys. Rev. E* **83**, 030303(R) (2011).

- [92] P. Olsson and S. Teitel, Dynamic length scales in athermal, shear-driven jamming of frictionless disks in two dimensions, *Phys. Rev. E* **102**, 042906 (2020).
- [93] K. Binder, M. Nauenberg, V. Privman, and A. P. Young, Finite-size tests of hyperscaling, *Phys. Rev. B* **31**, 1498 (1985).
- [94] M. Wittmann and A. P. Young, Finite-size scaling above the upper critical dimension, *Phys. Rev. E* **90**, 062137 (2014).
- [95] P. Charbonneau and P. K. Morse, Comment on “Explicit Analytical Solution for Random Close Packing in $d = 2$ and $d = 3$,” [arXiv:2201.07629](https://arxiv.org/abs/2201.07629).
- [96] Duke Digital Repository, <https://doi.org/10.7924/r4th8qc0b>.